

Bridging EUV and white-light observations: evidence for the breakout model in a “two-stage” solar eruptive event.

J. P. Byrne¹ · H. Morgan² · D. B. Seaton³ ·
H. M. Bain⁴ · S. R. Habbal¹

© Springer ••••

Abstract The initiation phase of CMEs is a very important aspect of solar physics, being an indication of the magnetic reconnection process that must be occurring to facilitate the shedding of helicity in the solar cycle. The interesting physics at play is known to occur between the photosphere and low corona, where many models introduce an instability that triggers a CME, often with associated flaring activity. To this end, it is important to obtain a variety of observations of the low corona in order to build as clear a picture as possible of the dynamics that occur therein. Here, we combine the EUV imagery of the SWAP instrument onboard *PROBA2* with the white-light imagery of the ground-based MK4 coronameter at MLSO in order to bridge the observational gap that exists between the disk imagery of AIA onboard *SDO* and the coronal imagery of LASCO onboard *SOHO*. Methods of multiscale image analysis were applied to the observations to better reveal the coronal signal while suppressing noise and other features. This allowed an investigation into the initiation phase of a CME that was driven by a rising flux rope structure from a “two-stage” flaring active region underlying an extended helmet streamer. It was found that the outward motion of the flux rope in the EUV observations led to a plasma pile-up of the white-light CME core material, while the overall system expanded into the helmet streamer to become the larger CME structure observed in the coronagraph images. Furthermore, the characterized CME core flux rope was determined to undergo a strong jerk in its motion, as the early acceleration jumped abruptly, simultaneous with the second-stage flaring and subsequent CME eruption through the LASCO field-of-view, which later became concave-outward in shape. These observations provide evidence for the breakout model, specifically in the case of a streamer blowout.

¹Institute for Astronomy, University of Hawai'i, 2680 Woodlawn Drive, Honolulu, HI 96822, USA. email:
jbyrne@ifa.hawaii.edu ²Sefydliad Mathemateg a Ffiseg, Prifysgol Aberystwyth, Ceredigion, Cymru, SY23 3BZ, UK.
³Royal Observatory of Belgium, Avenue Circulaire 3, 1180 Brussels, Belgium. ⁴Space Sciences Laboratory, University of California, Berkeley, CA 94720-7450, USA.

Keywords: Coronal Mass Ejections, Low Coronal Signatures, Initiation and Propagation

1. Introduction

Coronal mass ejections (CMEs) represent the largest, most dynamic phenomena that originate from the Sun. Propagating at speeds of hundreds up to thousands of kilometers per second (Yashiro *et al.*, 2004), the particle densities and energies involved can cause adverse space weather at Earth and elsewhere in the heliosphere (Schwenn *et al.*, 2005). They can lead to geomagnetic storms upon impacting our magnetosphere, damaging satellites, affecting communication and navigation systems, and increasing the radiation risk for astronauts (Lockwood and Hapgood, 2007). Given their potentially hazardous impact on Earth's geomagnetic environment, the physics governing their eruption and propagation needs to be understood.

Various theoretical CME models exist in the effort to reproduce the physical driver mechanisms responsible for their initiation and propagation (see the review by Chen, 2011). All are based upon the requirement that some form of instability must trigger the eruption, most likely as a result of a magnetic energy imbalance often described in the context of tether straining and release (Klimchuk, 2001). Considering the underlying structure of the CME as a flux rope (e.g., Chen, 1996), possible causes for eruption may include flux injection and magnetic twisting (Kliem and Török, 2006; Krall *et al.*, 2001), reconnection beneath the flux rope (Lin *et al.*, 2007; Amari *et al.*, 2003), or breakout reconnection between the overlying field and neighboring flux systems (Lynch *et al.*, 2008; van der Holst, Jacobs, and Poedts, 2007). Such models may provide an interpretation on observations, and thus allow some deeper understanding of the forces governing CMEs and their relationship with associated phenomena like flares.

An important aspect of studying CME initiation, is the ability to resolve their low-corona propagation and associated source regions on the disk: be it a flaring or non-flaring active region, a prominence/filament eruption or other rising loop system (Zhang and Wang, 2002; Subramanian and Dere, 2001), or else a “stealth CME” without any specifically detectable source (Howard and Harrison, 2013). Prominence lift-offs often become the core material of a CME (Filippov and Koutchmy, 2008; Gopalswamy *et al.*, 2003), and rising loops often form some part of the CME morphology (Dauphin, Vilmer, and Krucker, 2006; Cremades and Bothmer, 2004). Their low-corona kinematics and morphology provide insight into the early forces at play, and so a rigorous study of such phenomena is key to understanding the physics involved. However, a difficulty exists in studies of coronal structure that are prone to low signal-to-noise ratios in the observational data. Low-coronal white-light observations using a coronagraph are problematic due to the strong radial brightness gradient and issues with scattered light in the instrument, while extended EUV disk observations are problematic due to the strong drop-off in emission brightness with increasing coronal height. These common issues with solar observational data motivate the ongoing development

and use of advanced image processing techniques to suppress noise and enhance structures in the image data (Druckmüllerová, Morgan, and Habbal, 2011; Gallagher *et al.*, 2011; Pérez-Suárez *et al.*, 2011; Stenborg, Vourlidas, and Howard, 2008; Young and Gallagher, 2008; Morgan, Habbal, and Woo, 2006; Stenborg and Cobelli, 2003).

In Section 2 we describe the observations and use of multiscale image processing methods. In Section 3 we present a case-study of a flux rope that erupted on 8 March 2011, to provide deeper insight to the initiation phase of CMEs. A discussion of the interpretation of this study is presented in Section 4, and final conclusions in Section 5.

2. Observations & Techniques

In order to connect CMEs to their source regions, data from disk imagers such as the Sun Watcher using APS detectors and image Processing (SWAP; Seaton *et al.*, 2013, Halain *et al.*, 2013) onboard the second Projects for Onboard Autonomy (*PROBA2*; Santandrea *et al.*, 2013) and the Atmospheric Imaging Assembly (AIA; Lemen *et al.*, 2012) onboard the Solar Dynamics Observatory (*SDO*; Pesnell, Thompson, and Chamberlin, 2012), may be used in tandem with coronagraph observations. However, difficulties in the interpretation of the observed features arise due to the varying instrument specifications, particularly the limitations on their fields-of-view, image passbands, and cadences of observations. In order to bridge the gap between the EUV observations of the low corona and the white-light images of the upper corona, the SWAP imager was used in conjunction with the Mauna Loa Solar Observatory (MLSO) MK4 coronameter (Elmore *et al.*, 2003) to directly compare the observations of CMEs as they erupt through the overlapping fields-of-view (Fig. 1). This allows a direct correspondence of features in the EUV images with those in the white-light images, and can therefore provide new insight into the initial phases of CME eruption and acceleration.

Methods of multiscale image processing have been developed in recent years for use on coronagraph images to enhance the underlying structure. The fundamental idea behind these methods is to highlight details apparent on different scales within the data. Therefore, multiscale techniques provide an ability to remove small-scale features in images, essentially suppressing the noise such that the structures of interest can be revealed in greater detail. By applying them to coronagraph images, the morphology of CMEs as they propagate through the corona in a sequence of observations can be determined with better accuracy than previously possible (Byrne *et al.*, 2009, 2012).

Multiscale methods are now demonstrated for use on the MK4 coronameter and SWAP EUV imager, to provide insight to the low-coronal morphology of erupting structures that form CMEs. Details on the fundamental techniques are outlined in Young and Gallagher (2008) wherein the magnitude of the multiscale gradient is used to show the relative strength of the detected edges in the image structure at a particular scale of the multiscale decomposition (i.e., the strongest edges appear brightest). To further increase the signal-to-noise ratio

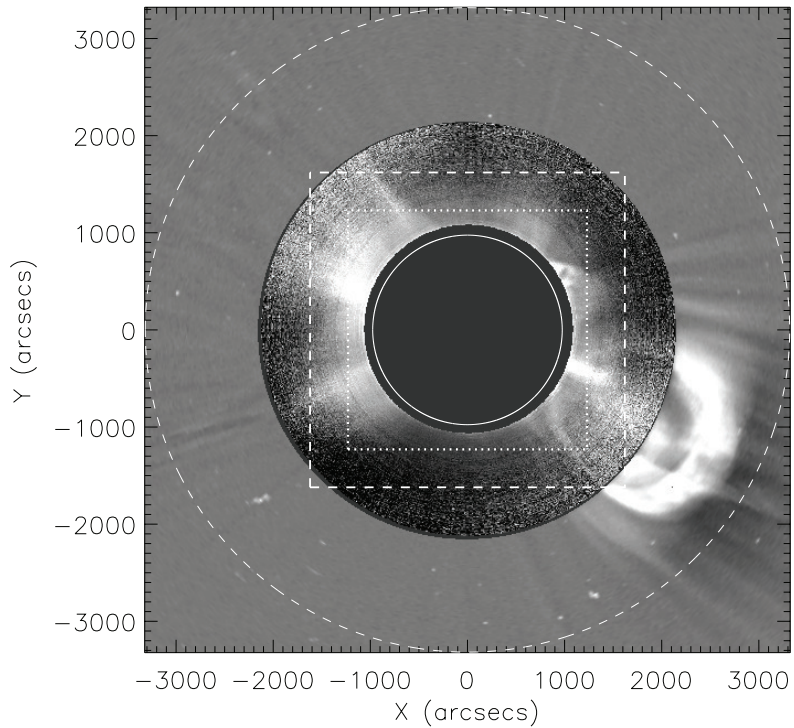


Figure 1. A LASCO/C2 image with an MLSO/MK4 image overlaid in the range $1.1\text{--}2.2 R_{\odot}$, dated 8 March 2011 at 20:24 and 20:22 UT respectively. The C2 image has been processed via the CORIMP techniques of normalizing radial graded filter (NRGF) and quiescent background subtraction. It has been trimmed to a half-width of $3.4 R_{\odot}$, which is the upper limit of the *PROBA2/SWAP* field-of-view as indicated by the dashed circle. The SWAP field-of-view during nominal operations is indicated by the dashed box. The *SDO/AIA* field-of-view is indicated by the inner dotted box. The limb of the Sun behind the occulter is indicated by the solid white circle. A CME is observed off the south-west limb as a bright loop structure with some inner core material, as seen here in the Thomson-scattered white-light coronagraph images. It is clear how the SWAP and AIA images can be used to bridge CME observations to the low corona and solar disk, for gaining insight to their initiation phase.

of the edge detections, the magnitude information from the scales most relevant to the coronal structures of interest may be multiplied together, neglecting the largest scales that smooth out the coronal signal, and the smallest scales that reveal the finer structure and noise (see Byrne *et al.*, 2012, for details). Thus the magnitude of the multiscale gradient across the dominant edges of coronal loops and CMEs is further enhanced for subsequent characterization of their morphology.

Figure 2 shows the effectiveness of the multiscale techniques for detecting the structure of an ejection observed by SWAP at 19:53:59 UT on 8 March 2011. The top left image shows the level-1 processed data, polar-unwrapped about Sun-center at coronal heights of $1\text{--}1.7 R_{\odot}$. The top right image shows the result of the multiscale filtering technique applied in such a manner as to enhance the edges

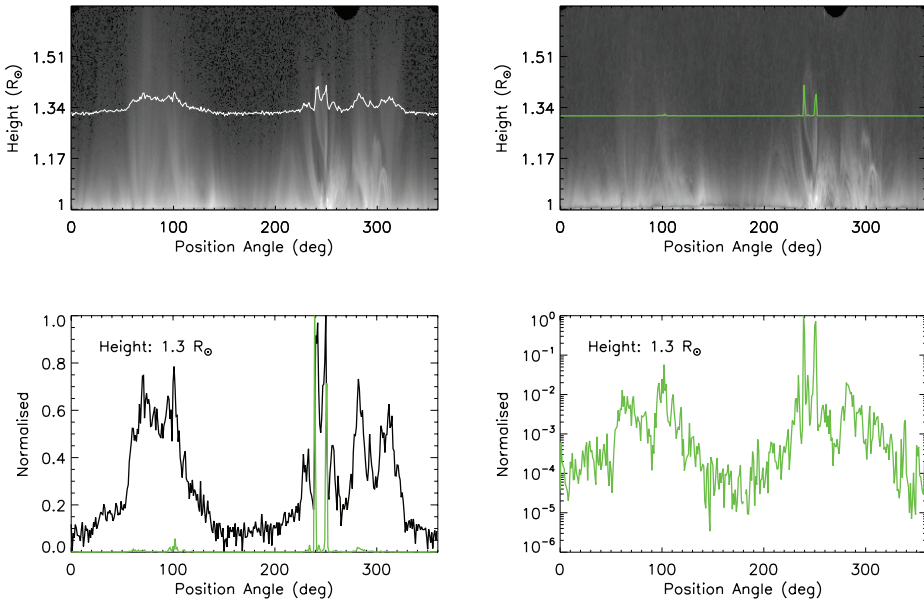


Figure 2. The top two panels show polar-unwrapped images of the solar corona across the *PROBA2/SWAP* field-of-view on 8 March 2011 at 19:53:59 UT; left being the level-1 data, right being the enhanced data (shown at log-scale image intensity). Across each image, at a constant height of $1.3 R_\odot$, a normalized intensity profile is plotted to demonstrate how the background coronal structure is suppressed by the multiscale techniques, to highlight only the complex structure of the prominence. The bottom left plot shows a direct comparison of the two intensity profiles, where the prominence is located between $230 - 260^\circ$. The bottom right plot shows a log scale of the normalized intensity profile across the enhanced image to demonstrate that the rest of the coronal structure is still present, just strongly suppressed relative to the prominence material.

of the detected structure in the data. The bottom left plot shows the comparison of a normalized intensity profile at a height of $1.3 R_\odot$ in each, revealing how the multiscale techniques best characterize the complex structure of the erupting prominence material located between $230 - 260^\circ$. The bottom right plot shows a log scale of the normalized intensity profile across the multiscale filtered image to reveal the suppressed signal of the background features.

The extended corona from $\sim 2 - 30 R_\odot$ is often observed with the Large Angle Spectrometric Coronagraph (LASCO; Brueckner *et al.*, 1995) onboard the Solar and Heliospheric Observatory (SOHO; Domingo, Fleck, and Poland, 1995) which orbits the L1 point. Coronal structures, and specifically CMEs, have been studied in the white-light image data from these instruments through the use of a number of steps outlined in the Coronal Image Processing package (CORIMP; Morgan, Byrne, and Habbal, 2012; Byrne *et al.*, 2012). These techniques have now been extended for use on the MLSO/MK4 coronameter data, which provides white-light polarization brightness images of the corona from $\sim 1.14 - 2.86 R_\odot$ at a cadence of approximately 3 minutes. The MK4 data is prepared via an instrumental vignetting function that maximizes the image contrast by offsetting the radial brightness gradient in order to best reveal structures such as CMEs and streamers. A multiscale decomposition is then performed in order

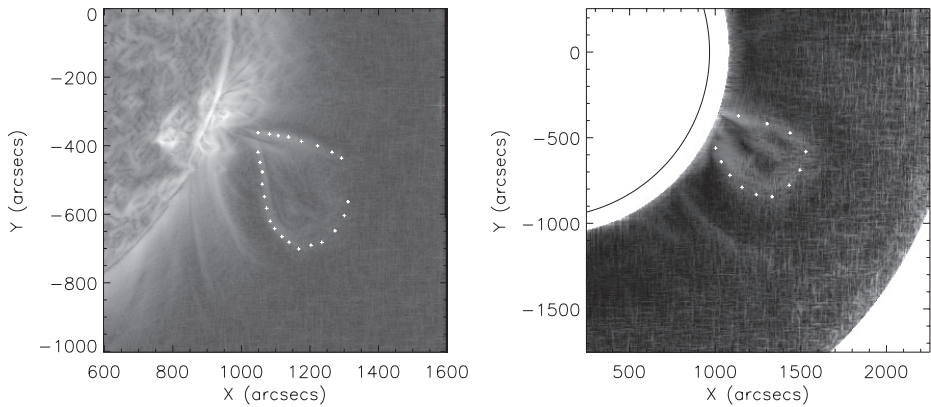


Figure 3. SWAP (left) and MK4 (right) observations of the erupting loop system that forms the core of the CME on 8 March 2011, at times 19:53:59 and 19:56:16 UT respectively. The images have been processed via the multiscale decomposition, with intensities that represent the relative magnitudes of the detected edges.

to produce magnitude images of the relative edge strengths in the image to highlight the detected structure (see Fig. 3). This allows, for example, an ellipse-fit characterization of the outward propagating fronts, as described in Byrne *et al.* (2009).

3. “Two-Stage” Solar Eruptive Event Case Study

A CME erupted from the southwest active region NOAA 11165 at approximately 19:30 UT on 8 March 2011. The active region caused numerous flares during its evolution across the disk, notably an M4.4 flare at GOES start-time 18:08 UT (peaking at 18:28 UT) associated with the rising loop system that later erupted to form the core material of the CME. Of particular interest for this event, is the “two-stage” X-ray flare profile seen in the GOES flux, identified as two individual M-class flares separated by almost 2 hours. Su *et al.* (2012) present this as clear evidence for a secondary heating phase. The loop system evolution was visible up to $\sim 1.3 R_\odot$ in AIA images, at which height a set of loops that were most strongly observed in AIA 171Å images began to erupt, coinciding with the time of the secondary M1.4 flare $\sim 20:00$ UT. These were then observable to a height of $\sim 1.6 R_\odot$ in the larger field-of-view of the SWAP 174Å imager. The observations of the active region are exhaustively reported by Su *et al.* (2012), though it is noted that the system of loops they track (see the stack plot in Fig. 4 of their paper) is not the same as the specific flux rope loops observed and tracked here, which erupted as the core of the CME (Fig. 4). The CME core is then observed in the white-light MK4 coronameter images to a height of $\sim 2.2 R_\odot$, entrained within a faint CME bubble that started to become visible at these heights before being clearly observed to propagate outwards in the extended LASCO coronagraph images. This type of cavity-CME morphology is often seen in low coronal observations, studied for example by Gibson *et al.*

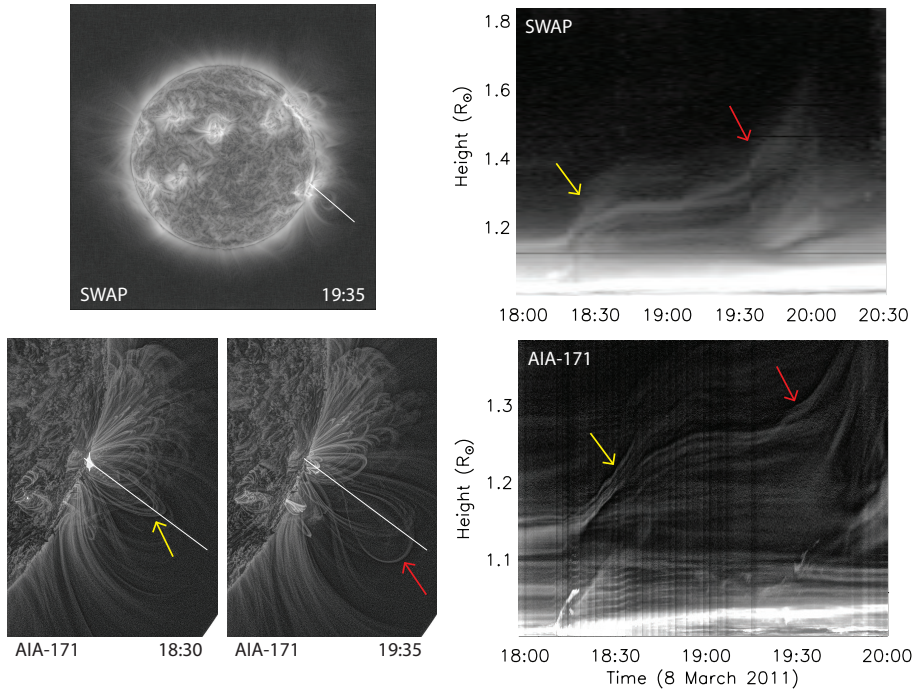


Figure 4. Stack plots were generated for a radial intensity profile through the SWAP and AIA-171 observations. The profile location is shown in a full field-of-view SWAP image at 19:35 UT (top left), and at two stages of the eruption in cropped AIA-171 images at 18:30 and 19:35 UT (bottom left). The stack plots (right) clearly show the two-stage eruption, with yellow and red arrows on the AIA images to indicate the different loop structures of interest; the latter of which becomes the CME core that is tracked through the SWAP, MK4 and LASCO observations. (An online animation accompanies this figure.)

(2006) for long-lasting structures seen in MK4 data, which erupt to become the typical three-part CME structure of a bright front, darker cavity and bright core Illing and Hundhausen (1986).

Morgan, Jeska, and Leonard (2013) report on the expansion of active region loops from this region into the extended solar corona in the few days leading up to this CME. The region lies beneath a helmet streamer structure that appears to contain the observed coronal loops, with a number of faint brightenings due to small outward-propagating plasma blobs. These, and the pointed shape of the rising loops, are postulated to be indicators of helmet streamer interchange reconnection at the apex of the closed field (Wang *et al.*, 2012). A subsequent brightening and expanding of the loops, accompanied by a swelling of the helmet streamer, precedes the CME from this region and is evidence for an energy input to the system that leads to an explosive energy release. Such a process manifests as the two-stage solar eruptive event outlined here and in the observations of Su *et al.* (2012). The AIA images of the active region underlying this system were processed with a multiscale Gaussian normalization technique (Morgan and Druckmüller, 2013) to enhance the observations of the coronal loop evolution over the course of the event. The right panels of Fig. 4 show stack plots obtained

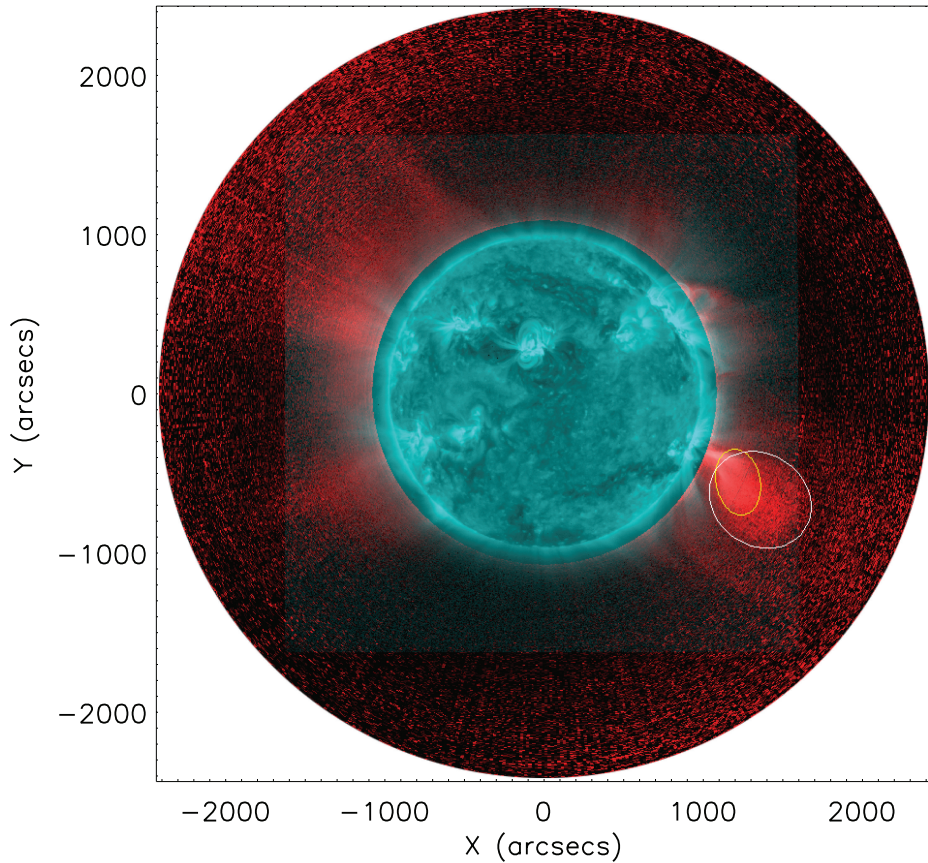


Figure 5. A merged SWAP (blue) and MK4 (red) image with the ellipse-fits to the characterized CME core material as observed by each instrument at 19:59 UT on 8 March 2011. (An online animation accompanies this figure.)

from a radial intensity profile through both the SWAP and AIA-171 observations, enhanced with the different multiscale filtering techniques. The stack plots clearly show the two stages of the eruption, with yellow and red arrows on the AIA images indicating the different loop structures that each intensity track corresponds to; the latter being the flux rope structure that erupts as the CME core.

In order to best reveal the eruption material when comparing the low signal-to-noise SWAP and MK4 images, multiscale methods of noise suppression and edge enhancement were employed, as discussed above. This allowed a robust point-&-click characterization of the CME core material, which was the brightest structure to be tracked through the different imagers when the CME front was not yet fully formed. The rising loop system observed with SWAP and the erupting CME core material observed with MK4 coincided both temporally and spatially, at least initially, and each was characterized by ellipse-fits to the detected front edges of the core flux-rope structure. Figure 5 shows an

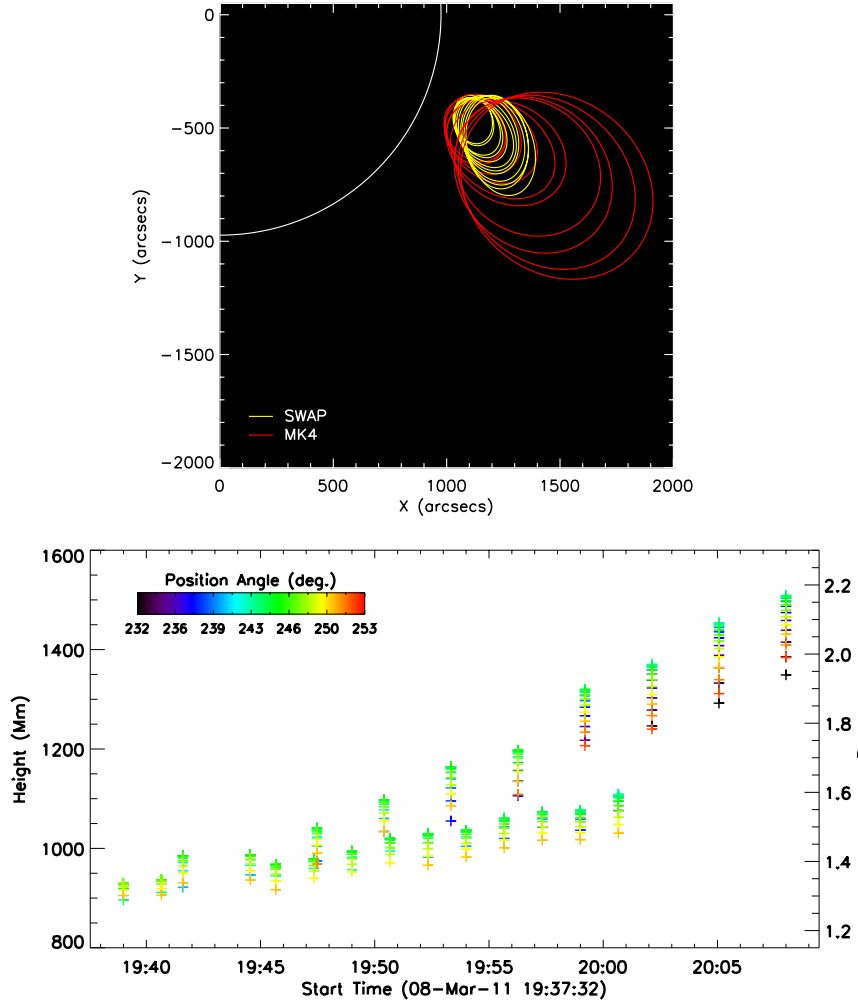


Figure 6. *Top:* The SWAP and MK4 ellipse-fits to the characterized CME core material over the course of the eruption. *Bottom:* The height-time profile of the characterized eruption observed simultaneously with the SWAP imager and MK4 coronameter. The erupting EUV loops move at a speed of $\sim 100 \text{ km s}^{-1}$ while the associated core of the resulting CME is observed to accelerate up to a speed of $\sim 400 \text{ km s}^{-1}$.

overlay of SWAP and MK4 images during the eruption at times 19:58:59 and 19:59:12 UT respectively, with the ellipse-fits to the erupting fronts. Figure 6 shows the progression of the ellipse-fits to the fronts over the course of the eruption, indicating how the white-light material observed with MK4 propagates away from the source quicker than the EUV material observed with SWAP. The different height-time profiles show the material in the MK4 images attained a speed of $\sim 400 \text{ km s}^{-1}$, while the associated erupting loop structures in the SWAP images moved at only $\sim 100 \text{ km s}^{-1}$.

The CME was observed to have a typical three-part structure that propagated out through the corona at a bulk speed in the range $\sim 400 - 600 \text{ km s}^{-1}$ (based on the kinematics of the CME front detected and tracked in the CORIMP catalog¹). The core of the CME was manually tracked via the multiscale methods and ellipse-fits discussed above (an example LASCO image is shown in Fig. 7). The resulting kinematics are plotted in Fig. 8, where the height-time measurements of the CME core are shown in color (corresponding to the position angle of the measurements across the plane-of-sky) overlaid on the CME front height-time measurements shown in gray for reference. The Savitzky-Golay filter is used to derive the velocity and acceleration profiles for the CME core; whereby a distribution of velocity and acceleration values is obtained at each data point, with the corresponding median, interquartile range, and upper and lower fences overlaid on each profile as solid, dashed and dotted lines respectively (see Byrne *et al.*, 2013 for a detailed discussion). The inset acceleration phase of the CME core shows initial values of approximately $\sim 20 \text{ m s}^{-2}$ jumping to $\sim 130 \text{ m s}^{-2}$, referred to as the CME jerk by Schrijver *et al.* (2008). The steepness of this jump may in part be attributed to the numerical effects of the data gap between MK4 and C2, where the spline-fit of the Savitzky-Golay filter (operating on a moving window of 6 neighboring data points) compensates somewhat for the jump in velocity that occurs between these two fields-of-view. The magnitude of the velocity, however, was verified by inspection of the different profiles within the separate instrument fields-of-view, for different degrees of polynomial fits and Savitzky-Golay filter sizes. That is, the rise in velocity is determined to be real, though its true steepness might be better quantified if it were possible to obtain a more complete set of measurements. Nevertheless, it occurs in sync with the second rise in the X-ray flare profile, being an indication of a very fast energy release that allows the explosive eruption of the CME to begin, before later attaining a speed akin to the local solar wind speed. This double acceleration profile is further evidence for the complexity of the system whose morphology has been observed to change dramatically over the course of its evolution (Morgan, Jeska, and Leonard, 2013; Su *et al.*, 2012).

4. Discussion

The study of this particular event is especially interesting in the context of the flare-CME relationship. The two-stage flaring profile of the erupting loop system is evidence for a secondary heating process (see (Su *et al.*, 2012) for details), indicating two stages of magnetic reconnection that occur to first change the topology of the system and then allow for the subsequent flux rope eruption. This scenario demonstrates that a loss of stability occurs initially, to allow the loop system to rise and alter its magnetic configuration with an explosive energy release detected as an M-class flare. This is followed by a secondary energy release that allows the underlying flux rope to erupt through the corona as a

¹<http://dublin.ifa.hawaii.edu/~jbyrne/CORIMP/>

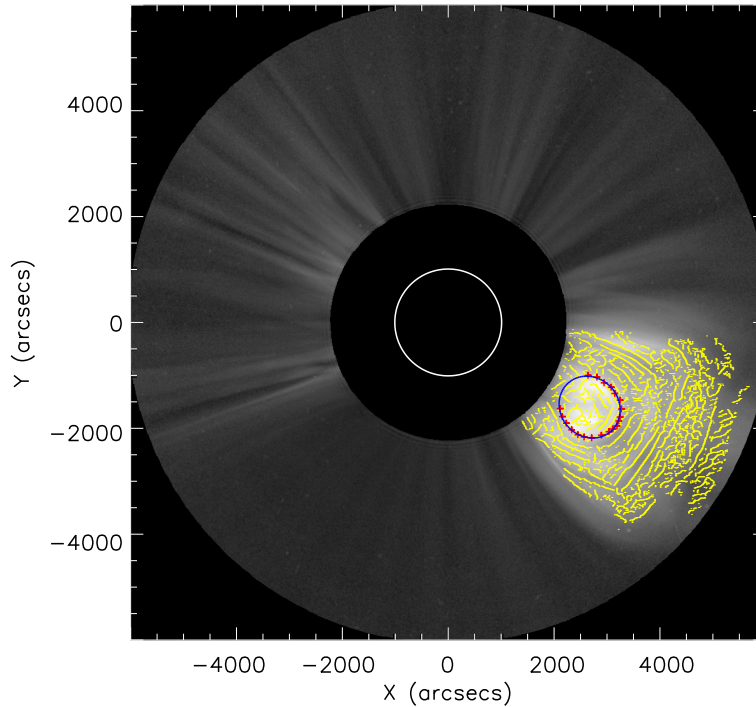


Figure 7. A radially filtered LASCO/C2 image of the CME at 21:06:51 UT on 8 March 2011. The yellow contours trace the edges in the detected CME structure (from the CORIMP catalog), with red points clicked along the corresponding core material, and a resulting ellipse-fit in blue.

CME, with the production of a second X-ray peak and post-flare loops at the CME footpoints.

It is not clear why we observe different rates of motion of the material in the SWAP and MK4 images during the CME onset (Fig. 6). The simplest reason is possibly that the material observed by the different instruments corresponds to different parts of the erupting structure that are difficult to dissociate from each other on the plane-of-sky. This could mean that line-of-sight effects are causing a discrepancy in the height-time profiles that appears as this offset in their rates of propagation. However, being a limb event, this seems too weak an argument for the large offset in the heights measured. While some cause for the offset may be attributed to a loss of signal in the EUV as the eruption proceeds to the edge of the field-of-view (diminishing in its signal-to-noise ratio), such an effect would not be strong enough to explain a consistently increasing offset of this magnitude since it would be expected that the white-light signal would undergo a similar effect in the MK4 observations. Indeed if the offset is true and the different parts of the structure (EUV emitting material versus white-light scattering material) do undergo different rates of propagation on the same plane-of-sky, it may be that the trailing part simply becomes a different portion of the

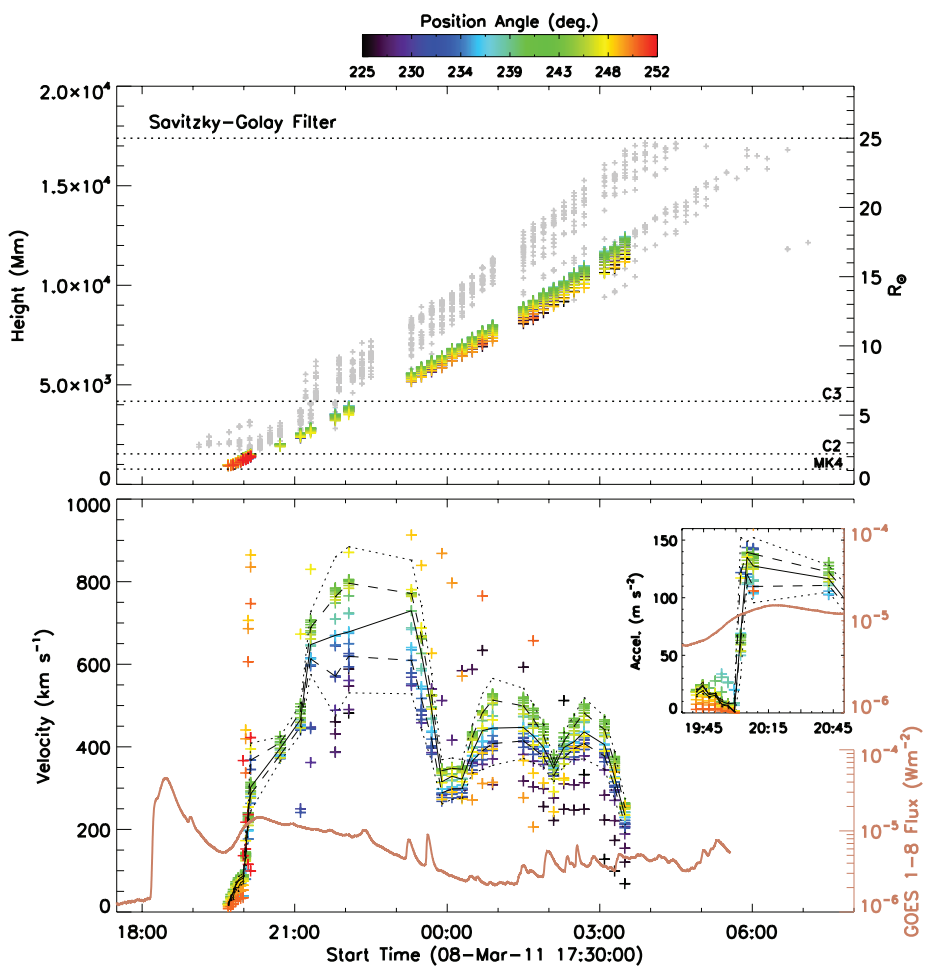


Figure 8. The kinematic profiles of height, velocity, and (inset) the early acceleration phase of the CME core material, detected and characterized via the multiscale edge enhancement and ellipse-fits (see Section 2 and Figs. 6 and 7). The automated CORIMP CME detections provide the height-time measurements shown here in gray for reference, with the characterized CME core height-time measurements plotted in color according to their position angle. The fields-of-view of the MK4, C2 and C3 instruments are indicated by the horizontal dotted lines, covering a useable range of $1.1 - 25 R_{\odot}$, with the CME core tracked to approximately $18 R_{\odot}$. A Savitzky-Golay filter was applied to the height-time measurements to obtain distribution profiles of velocity and acceleration, with the median, interquartiles range, and upper/lower fences over-plotted in solid, dashed and dotted lines respectively. Overlaid is the GOES X-ray $1 - 8 \text{ \AA}$ flux profile, showing the double-eruption peaks at about 18:28 and 20:15 UT, the latter of which coincides with the CME jerk (jump in acceleration).

main CME and/or undergoes a delayed jerk in its motion, which is not observed as the EUV signal diminishes towards the edge of the SWAP field-of-view. This would imply that there is some form of delayed or staggered eruption occurring throughout the CME structure, or that an expansion effect takes over as the CME bubble forms, that acts to create the observed offset between the different observations.

More intriguing is the possibility that this event is a good example of a breakout CME. The observations of Morgan, Jeska, and Leonard (2013) show a streamer swelling on the limb above the active region to large heights in the LASCO coronagraphs, that evolves slowly over the preceding days in the lead-up to the eruptive event; and being disturbed by an earlier CME that erupts to the northwest on March 7, and some faint brightenings and outward propagating blobs within the expanding helmet streamer loops indicative of interchange reconnection. Helmet streamers have long been recognized as an observational precursor to CME initiation (Hundhausen, 1993) though not always observed to such heights due to the low signal-to-noise ratio, overcome by the dynamic separation technique of Morgan, Byrne, and Habbal (2012). For this active region it may be postulated that a form of reconnection is occurring in the helmet streamer in the lead-up to, and most strongly at, the time of the main flare (M4.4; \sim 18:08 UT) that allows a change in the magnetic topology of the system such that the CME flux rope can form and then erupt at the time of the secondary flare (M1.4; \sim 20:00 UT). These observations suggest a form of breakout reconnection is driving the streamer blowout CME as modeled by van der Holst *et al.* (2009), wherein they describe how the rising flux rope can “snow plow” the plasma ahead of it. This has the effect of broadening the helmet streamer and facilitating breakout reconnection between the flux rope and the helmet field. Flare reconnection then sets in due to the expansion of the magnetic field in the wake of the erupting breakout arcade. These effects could account for the combined observations of this event; most notably the offset in the flux rope motion observed in EUV and the plasma motion observed in white-light, that form the core of the CME whose increased size may be attributed to the helmet streamer blowout. The measured jerk in the CME motion then coincides with the allowed blowout eruption through the breakout process, while reconnection occurs behind as indicated by the elongated “X”-shaped structure and post-flare loops in the observations of Su *et al.* (2012).

5. Conclusions

The *PROBA2/SWAP* imager is unique in that it provides extended EUV observations of the Sun and low-corona to greater heights than other EUV imagers such as *SDO/AIA*. An ongoing goal in solar physics has been to study the connection between processes on the Sun and the effects felt elsewhere in the heliosphere; a connection known to lie predominantly between the regions of the photosphere, chromosphere and corona. Therefore obtaining extensive observations across the solar atmosphere is paramount to understanding the physics at play. Since the LASCO/C1 coronagraph was lost very early on in the *SOHO* mission, observations of the low corona have generally been quite limited. In order to bridge this gap and garner some knowledge of the low-corona initiation phase of CMEs, we have combined the SWAP observations with those of the ground-based MK4 coronameter, to directly compare the EUV and white-light imagery. This was achieved through the use of advanced image processing techniques to overcome the low signal-to-noise ratio in these data, and characterize

the erupting structures of interest. The subsequent investigation of the dynamics of a specific case-study on 8 March 2011 provides insight to the early CME formation and eruption, using SWAP and MK4 in tandem with the observations of AIA and LASCO. This complements the previous investigation of Su *et al.* (2012) who first reported on the event's two-stage flaring profile as evidence for secondary heating, and provides direct evidence for the breakout model, specifically in the case of a streamer blowout. The helmet streamer evolution ahead of the flare, the "two-stage" flaring profile, and abrupt CME acceleration onset, all indicate breakout reconnection as the mechanism of eruption, especially in light of the subsequent CME and helmet evolution through the corona. Our study highlights the importance of multi-wavelength, high-cadence, extensive coverage observations of the low-corona, where the physical mechanisms that underly CME formation, initiation, and connection with flares and surrounding coronal field may best be investigated. It is hoped that future instruments such as the new COSMO K-coronagraph² will help to advance this.

Acknowledgements This work is supported by SHINE grant 0962716 and NASA grants NNX08AJ07G and NNX13AG11G to the Institute for Astronomy. SWAP is a project of the Centre Spatial de Liège and the Royal Observatory of Belgium funded by the Belgian Federal Science Policy Office (BELSPO). MK4 data is provided courtesy of the Mauna Loa Solar Observatory, operated by the High Altitude Observatory, as part of the National Center for Atmospheric Research (NCAR). NCAR is supported by the National Science Foundation. The *SOHO*/LASCO data used here are produced by a consortium of the Naval Research Laboratory (USA), Max-Planck-Institut für Aeronomie (Germany), Laboratoire d'Astronomie (France), and the University of Birmingham (UK). SOHO is a project of international cooperation between ESA and NASA. *SDO* data supplied courtesy of the NASA/*SDO* consortia. JPB is grateful to have been a PROBA2 Guest Investigator.

References

- Amari, T., Luciani, J.F., Aly, J.J., Mikic, Z., Linker, J.: 2003, Coronal Mass Ejection: Initiation, Magnetic Helicity, and Flux Ropes. II. Turbulent Diffusion-driven Evolution. *Astrophysical Journal* **595**, 1231–1250. doi:10.1086/377444.
- Brueckner, G.E., Howard, R.A., Koomen, M.J., Korendyke, C.M., Michels, D.J., Moses, J.D., Socker, D.G., Dere, K.P., Lamy, P.L., Llebaria, A., Bout, M.V., Schwenn, R., Simnett, G.M., Bedford, D.K., Eyles, C.J.: 1995, The Large Angle Spectroscopic Coronagraph (LASCO). *Solar Physics* **162**, 357–402. doi:10.1007/BF00733434.
- Byrne, J.P., Gallagher, P.T., McAteer, R.T.J., Young, C.A.: 2009, The kinematics of coronal mass ejections using multiscale methods. *Astronomy & Astrophysics* **495**, 325–334. doi:10.1051/0004-6361:200809811.
- Byrne, J.P., Morgan, H., Habbal, S.R., Gallagher, P.T.: 2012, Automatic Detection and Tracking of Coronal Mass Ejections. II. Multiscale Filtering of Coronagraph Images. *Astrophysical Journal* **752**, 145. doi:10.1088/0004-637X/752/2/145.
- Byrne, J.P., Long, D.M., Gallagher, P.T., Bloomfield, D.S., Maloney, S.A., McAteer, R.T.J., Morgan, H., Habbal, S.R.: 2013, Improved methods for determining the kinematics of coronal mass ejections and coronal waves. *Astronomy & Astrophysics* **557**, A96. doi:10.1051/0004-6361/201321223.
- Chen, J.: 1996, Theory of prominence eruption and propagation: Interplanetary consequences. *Journal of Geophysical Research* **101**, 27499–27520. doi:10.1029/96JA02644.
- Chen, P.F.: 2011, Coronal Mass Ejections: Models and Their Observational Basis. *Living Reviews in Solar Physics* **8**, 1.

²<http://www.cosmo.ucar.edu/kcoronagraph.html>

- Cremades, H., Bothmer, V.: 2004, On the three-dimensional configuration of coronal mass ejections. *Astronomy & Astrophysics* **422**, 307–322. doi:10.1051/0004-6361:20035776.
- Dauphin, C., Vilmer, N., Krucker, S.: 2006, Observations of a soft X-ray rising loop associated with a type II burst and a coronal mass ejection in the 03 November 2003 X-ray flare. *Astronomy & Astrophysics* **455**, 339–348. doi:10.1051/0004-6361:20054535.
- Domingo, V., Fleck, B., Poland, A.I.: 1995, The SOHO Mission: an Overview. *Solar Physics* **162**, 1–2. doi:10.1007/BF00733425.
- Druckmüllerová, H., Morgan, H., Habbal, S.R.: 2011, Enhancing Coronal Structures with the Fourier Normalizing-radial-graded Filter. *Astrophysical Journal* **737**, 88. doi:10.1088/0004-637X/737/2/88.
- Elmore, D.F., Burkepile, J.T., Darnell, J.A., Lecinski, A.R., Stanger, A.L.: 2003, Calibration of a ground-based solar coronal polarimeter. In: Fineschi, S. (ed.) *Society of Photo-Optical Instrumentation Engineers (SPIE) Conference Series, Society of Photo-Optical Instrumentation Engineers (SPIE) Conference Series* **4843**, 66–75. doi:10.1117/12.459279.
- Filippov, B., Koutchmy, S.: 2008, Causal relationships between eruptive prominences and coronal mass ejections. *Annales Geophysicae* **26**, 3025–3031. doi:10.5194/angeo-26-3025-2008.
- Gallagher, P.T., Young, C.A., Byrne, J.P., McAtee, R.T.J.: 2011, Coronal mass ejection detection using wavelets, curvelets and ridgelets: Applications for space weather monitoring. *Advances in Space Research* **47**, 2118–2126. doi:10.1016/j.asr.2010.03.028.
- Gibson, S.E., Foster, D., Burkepile, J., de Toma, G., Stanger, A.: 2006, The Calm before the Storm: The Link between Quiescent Cavities and Coronal Mass Ejections. *Astrophysical Journal* **641**, 590–605. doi:10.1086/500446.
- Gopalswamy, N., Shimojo, M., Lu, W., Yashiro, S., Shibasaki, K., Howard, R.A.: 2003, Prominence Eruptions and Coronal Mass Ejection: A Statistical Study Using Microwave Observations. *Astrophysical Journal* **586**, 562–578. doi:10.1086/367614.
- Halain, J.-P., Berghmans, D., Seaton, D.B., Nicula, B., De Groof, A., Mierla, M., Mazzoli, A., Defise, J.-M., Rochus, P.: 2013, The SWAP EUV Imaging Telescope. Part II: In-flight Performance and Calibration. *Solar Physics* **286**, 67–91. doi:10.1007/s11207-012-0183-6.
- Howard, T.A., Harrison, R.A.: 2013, Stealth Coronal Mass Ejections: A Perspective. *Solar Physics* **285**, 269–280. doi:10.1007/s11207-012-0217-0.
- Hundhausen, A.J.: 1993, Sizes and locations of coronal mass ejections - SMM observations from 1980 and 1984–1989. *Journal of Geophysical Research* **98**, 13177. doi:10.1029/93JA00157.
- Illing, R.M.E., Hundhausen, A.J.: 1986, Disruption of a coronal streamer by an eruptive prominence and coronal mass ejection. *Journal of Geophysical Research* **91**, 10951–10960. doi:10.1029/JA091iA10p10951.
- Kliem, B., Török, T.: 2006, Torus Instability. *Physical Review Letters* **96**(25), 255002. doi:10.1103/PhysRevLett.96.255002.
- Klimchuk, J.A.: 2001, Theory of Coronal Mass Ejections. *Space Weather (Geophysical Monograph 125)*, ed. P. Song, H. Singer, G. Siscoe (Washington: Am. Geophys. Un.) **125**, 143.
- Krall, J., Chen, J., Duffin, R.T., Howard, R.A., Thompson, B.J.: 2001, Erupting Solar Magnetic Flux Ropes: Theory and Observation. *Astrophysical Journal* **562**, 1045–1057. doi:10.1086/323844.
- Lemen, J.R., Title, A.M., Akin, D.J., Boerner, P.F., Chou, C., Drake, J.F., Duncan, D.W., Edwards, C.G., Friedlaender, F.M., Heyman, G.F., Hurlburt, N.E., Katz, N.L., Kushner, G.D., Levay, M., Lindgren, R.W., Mathur, D.P., McFeaters, E.L., Mitchell, S., Rehse, R.A., Schrijver, C.J., Springer, L.A., Stern, R.A., Tarbell, T.D., Wuelser, J.-P., Wolfson, C.J., Yanari, C., Bookbinder, J.A., Cheimets, P.N., Caldwell, D., Deluca, E.E., Gates, R., Golub, L., Park, S., Podgorski, W.A., Bush, R.I., Scherrer, P.H., Gummin, M.A., Smith, P., Aufer, G., Jerram, P., Pool, P., Soufli, R., Windt, D.L., Beardsley, S., Clapp, M., Lang, J., Waltham, N.: 2012, The Atmospheric Imaging Assembly (AIA) on the Solar Dynamics Observatory (SDO). *Solar Physics* **275**, 17–40. doi:10.1007/s11207-011-9776-8.
- Lin, J., Li, J., Forbes, T.G., Ko, Y., Raymond, J.C., Vourlidas, A.: 2007, Features and Properties of Coronal Mass Ejection/Flare Current Sheets. *Astrophysical Journal Letters* **658**, L123–L126. doi:10.1086/515568.
- Lockwood, M., Hapgood, M.: 2007, The Rough Guide to the Moon and Mars. *Astronomy and Geophysics* **48**(6), 060000–6. doi:10.1111/j.1468-4004.2007.48611.x.
- Lynch, B.J., Antiochos, S.K., DeVore, C.R., Luhmann, J.G., Zurbuchen, T.H.: 2008, Topological Evolution of a Fast Magnetic Breakout CME in Three Dimensions. *Astrophysical Journal* **683**, 1192–1206. doi:10.1086/589738.

- Morgan, H., Druckmüller, M.: 2013, Multi-scale Gaussian normalization for image processing: application to solar EUV observations. *Solar Physics (in review)*.
- Morgan, H., Byrne, J.P., Habbal, S.R.: 2012, Automatically Detecting and Tracking Coronal Mass Ejections. I. Separation of Dynamic and Quiescent Components in Coronagraph Images. *Astrophysical Journal* **752**, 144. doi:10.1088/0004-637X/752/2/144.
- Morgan, H., Habbal, S.R., Woo, R.: 2006, The Depiction of Coronal Structure in White-Light Images. *Solar Physics* **236**, 263–272. doi:10.1007/s11207-006-0113-6.
- Morgan, H., Jeska, L., Leonard, D.: 2013, The Expansion of Active Regions into the Extended Solar Corona. *Astrophysical Journal Supplement* **206**, 19. doi:10.1088/0067-0049/206/2/19.
- Pérez-Suárez, D., Higgins, P.A., Bloomfield, D.S., McAteer, R.T.J., Krista, L.D., Byrne, J.P., Gallagher, P.T.: 2011, "Automated Solar Feature Detection for Space Weather Applications", in *Applied Signal and Image Processing: Multidisciplinary Advancements*, eds. R. Qahwaji, R. Green, & E. L. Hines, (IGI Global), p. 207–225.
- Pesnell, W.D., Thompson, B.J., Chamberlin, P.C.: 2012, The Solar Dynamics Observatory (SDO). *Solar Physics* **275**, 3–15. doi:10.1007/s11207-011-9841-3.
- Santandrea, S., Gantois, K., Straub, K., Teston, F., Tilmans, E., Baijot, C., Gerrits, D., De Groof, A., Schwemmer, G., Zender, J.: 2013, PROBA2: Mission and Spacecraft Overview. *Solar Physics* **286**, 5–19. doi:10.1007/s11207-013-0289-5.
- Schrijver, C.J., Elmore, C., Kliem, B., Török, T., Title, A.M.: 2008, Observations and Modeling of the Early Acceleration Phase of Erupting Filaments Involved in Coronal Mass Ejections. *Astrophysical Journal* **674**, 586–595. doi:10.1086/524294.
- Schwenn, R., dal Lago, A., Huttunen, E., Gonzalez, W.D.: 2005, The association of coronal mass ejections with their effects near the Earth. *Annales Geophysicae* **23**, 1033–1059.
- Seaton, D.B., Berghmans, D., Nicula, B., Halain, J.-P., De Groof, A., Thibert, T., Bloomfield, D.S., Raftery, C.L., Gallagher, P.T., Auchère, F., Defise, J.-M., D'Huys, E., Lecat, J.-H., Mazy, E., Rochus, P., Rossi, L., Schühle, U., Slemzin, V., Yalim, M.S., Zender, J.: 2013, The SWAP EUV Imaging Telescope Part I: Instrument Overview and Pre-Flight Testing. *Solar Physics* **286**, 43–65. doi:10.1007/s11207-012-0114-6.
- Stenborg, G., Cobelli, P.J.: 2003, A wavelet packets equalization technique to reveal the multi-scale spatial nature of coronal structures. *Astronomy & Astrophysics* **398**, 1185–1193. doi:10.1051/0004-6361:20021687.
- Stenborg, G., Vourlidas, A., Howard, R.A.: 2008, A Fresh View of the Extreme-Ultraviolet Corona from the Application of a New Image-Processing Technique. *Astrophysical Journal* **674**, 1201–1206. doi:10.1086/525556.
- Su, Y., Dennis, B.R., Holman, G.D., Wang, T., Chamberlin, P.C., Savage, S., Veronig, A.: 2012, Observations of a Two-stage Solar Eruptive Event (SEE): Evidence for Secondary Heating. *Astrophysical Journal Letters* **746**, L5. doi:10.1088/2041-8205/746/1/L5.
- Subramanian, P., Dere, K.P.: 2001, Source Regions of Coronal Mass Ejections. *Astrophysical Journal* **561**, 372–395. doi:10.1086/323213.
- van der Holst, B., Jacobs, C., Poedts, S.: 2007, Simulation of a Breakout Coronal Mass Ejection in the Solar Wind. *Astrophysical Journal Letters* **671**, L77–L80. doi:10.1086/524732.
- van der Holst, B., Manchester, W. IV, Sokolov, I.V., Tóth, G., Gombosi, T.I., DeZeeuw, D., Cohen, O.: 2009, Breakout Coronal Mass Ejection or Streamer Blowout: The Bugle Effect. *Astrophysical Journal* **693**, 1178–1187. doi:10.1088/0004-637X/693/2/1178.
- Wang, Y.-M., Grappin, R., Robbrecht, E., Sheeley, N.R. Jr.: 2012, On the Nature of the Solar Wind from Coronal Pseudostreamers. *Astrophysical Journal* **749**, 182. doi:10.1088/0004-637X/749/2/182.
- Yashiro, S., Gopalswamy, N., Michalek, G., St. Cyr, O.C., Plunkett, S.P., Rich, N.B., Howard, R.A.: 2004, A catalog of white light coronal mass ejections observed by the SOHO spacecraft. *Journal of Geophysical Research (Space Physics)* **109**, 7105. doi:10.1029/2003JA010282.
- Young, C.A., Gallagher, P.T.: 2008, Multiscale Edge Detection in the Corona. *Solar Physics* **248**, 457–469. doi:10.1007/s11207-008-9177-9.
- Zhang, J., Wang, J.: 2002, Are Homologous Flare-Coronal Mass Ejection Events Triggered by Moving Magnetic Features? *Astrophysical Journal* **566**, L117–L120. <http://adsabs.harvard.edu/abs/2002ApJ...566L.117Z>.